The CD20 homologue MS4A4 directs trafficking of KIT toward clathrin-independent endocytosis pathways and thus regulates receptor signaling and recycling

Glenn Cruse[a], Michael A. Beaven[b], Stephen C. Music[a], Peter Bradding[c], Alasdair M. Gilfillan[a], and Dean D. Metcalfe[a]

[a]Laboratory of Allergic Diseases, National Institute of Allergy and Infectious Diseases and [b]Laboratory of Molecular Immunology, National Heart, Lung and Blood Institute, National Institutes of Health, Bethesda, MD 20892; [c]Department of Infection, Immunity and Inflammation, Institute for Lung Health, University of Leicester, Glenfield Hospital, Leicester LE3 9QP, United Kingdom

ABSTRACT MS4A family members differentially regulate the cell cycle, and aberrant, or loss of, expression of MS4A family proteins has been observed in colon and lung cancer. However, the precise functions of MS4A family proteins and their mechanistic interactions remain unsolved. Here we report that MS4A4 facilitates trafficking of the receptor tyrosine kinase KIT through endocytic recycling rather than degradation pathways by a mechanism that involves recruitment of KIT to caveolin-1–enriched microdomains. Silencing of MS4A4 in human mast cells altered ligand-induced KIT endocytosis pathways and reduced receptor recycling to the cell surface, thus promoting KIT signaling in the endosomes while reducing that in the plasma membrane, as exemplified by Akt and PLCγ1 phosphorylation, respectively. The altered endocytic trafficking of KIT also resulted in an increase in SCF-induced mast cell proliferation and migration, which may reflect altered signaling in these cells. Our data reveal a novel function for MS4A family proteins in regulating trafficking and signaling, which could have implications in both proliferative and immunological diseases.

INTRODUCTION

The membrane-spanning the 4A (MS4A) gene family is clustered within chromosome 11q12-q13 and encodes a family of proteins with similar topology to tetraspanins (Ishibashi *et al.*, 2001; Liang *et al.*, 2001; Liang and Tedder, 2001). The MS4A genes are expressed predominately in immune cells, and human linkage analyses have identified that the gene loci 11q12-q13 are strongly linked to allergy and asthma susceptibility. *MS4A1* (encoding CD20) and

MS4A2 (encoding the β subunit of the high-affinity immunoglobulin E receptor FcεRI) are associated with the activation and proliferation of B cells (Tedder and Engel, 1994) and mast cells (MCs) (Kraft *et al.*, 2004; Cruse *et al.*, 2010, 2013), respectively, and are therefore considered potential candidates for allergy and asthma susceptibility.

In addition to their potential link to asthma and inflammatory diseases, MS4A family members are also reported to regulate the cell cycle (Donato *et al.*, 2002; Cruse *et al.*, 2010; Xu *et al.*, 2010; Kutok *et al.*, 2011), and aberrant or loss of expression of MS4A proteins has been observed in cancers of the colon, lung, and other tissues (Bangur *et al.*, 2004; Koslowski *et al.*, 2008; Dalerba *et al.*, 2011; Kutok *et al.*, 2011; Michel *et al.*, 2013). Further, genome-wide association studies have linked both MS4A4 and MS4A6 to the development of late-onset Alzheimer's disease (Hollingworth *et al.*, 2011; Naj *et al.*, 2011). However, because the function of the MS4A proteins is unknown, the consequences of their aberrant expression in cancer development or other disease states are unclear.

We undertook studies of the MS4A proteins in MCs because of their linkage to allergic diseases. We reported on novel roles of a

Abbreviations used: EE, early endosome; ERC, endocytic recycling compartment; IF, immunofluorescence; KIT, stem cell factor receptor; LE, late endosome; MC, mast cell; MS4A, membrane-spanning 4A; SCF, stem cell factor.

truncated variant of MS4A2 in facilitating IgE receptor (FcεRI)–mediated, Ca^{2+}-dependent microtubule assembly and degranulation in MCs (Cruse *et al.*, 2013). We now report that another MS4A family member, MS4A4, regulates MC function by promoting surface expression of the receptor tyrosine kinase (RTK) stem cell factor receptor (KIT), an essential receptor for MC maturation and function (Okayama and Kawakami, 2006; Jensen *et al.*, 2007). MS4A4 also regulates signaling through the phospholipase C γ1 (PLCγ1) pathway for KIT, possibly by recruitment of receptors to lipid rafts. Altered KIT trafficking and signaling with MS4A4 silencing resulted in an increase in AKT signaling and MC proliferation. These findings imply that MS4A4 dysfunction in MCs may result in aberrant cellular responses and may help explain the observations that aberrant genetic expression of MS4A family members is associated with a range of disease processes.

RESULTS

Human MCs express MS4A4 mRNA

The *MS4A4A* gene produces at least three known MS4A4 splice variants in humans (Supplemental Figure S1). To determine whether MS4A4 mRNA was expressed in human mast cells, we designed primers that would amplify all variants. We observed that MS4A4 mRNA was expressed in primary human lung MCs (HLMCs; Figure 1A). MS4A4 mRNA was also expressed in human MCs derived from peripheral blood CD34^{+} progenitors (HuMCs), the transformed human MC line, LAD-2, and to a lesser extent in the HMC-1.1 and HMC-1.2 human MC lines (Figure 1, B and C). Expression of MS4A4 mRNA increased during culture of MC precursors from peripheral blood, especially as MCs reached maturity at 8 wk (Figure 1D).

On examining the effects of gene silencing of MS4A4 using four different short hairpin RNA (shRNA) constructs in LAD-2 cells, we found all to reduce substantially MS4A4 mRNA expression (Figure 1E). Silencing MS4A4 with shMS4A4v4 also reduced protein expression (~50%) when examined using flow cytometry (Figure 1, F and G).

Silencing MS4A4 alters surface expression of KIT

We next examined the expression of surface KIT using flow cytometry, given the key role that the KIT ligand, stem cell factor (SCF), plays in maintaining MC viability and function. A marked reduction in KIT on the cell surface was observed with all shMS4A4 constructs (Figure 1H). Examination of total KIT protein expression in fixed and permeabilized LAD-2 cells revealed that silencing MS4A4 also resulted in a comparable reduction in both surface and total KIT expression compared with control cells (compare Figure 1, I to J). This suggests that the reduced receptor expression could be due to increased internalization and degradation. Expression of another MC surface marker, the intercellular adhesion molecule 1 (ICAM-1 [CD54]), was unaffected (Figure 1K). The reduction in surface KIT expression correlated with relative MS4A4 mRNA expression after transduction with all shMS4A4 constructs (compare Figure 1, E and H). Therefore the reduction in KIT surface expression appeared to be directly related to the reduced expression of MS4A4. Because there was no reduction in KIT mRNA expression (Figure 1L) as determined by quantitative PCR and no correlation between surface KIT and relative KIT mRNA expression (Figure 1M), it would appear that MS4A4 contributes to surface KIT expression by regulating trafficking and/or degradation pathways rather than down-regulating *c-KIT* transcription.

Measurement of cell viability and apoptosis indicated that three of the shMS4A4 constructs reduced cell viability and increased surface annexin V expression. However, shMS4A4v4 had no cytotoxic effects (Figure 1N), silenced MS4A4 with equal efficiency to the other constructs (Figure 1E), and also reduced KIT expression to the same degree (Figure 1H). Therefore shMS4A4v4 was selected for further studies.

### MS4A4 regulates KIT endocytosis and recycling to the plasma membrane

To examine whether MS4A4 promotes trafficking of KIT to the plasma membrane, we removed SCF from the cultures to stop ligand-induced KIT internalization. Measurement of surface KIT on LAD-2 cells in the continuous presence of SCF in culture revealed a marked reduction in surface KIT in MS4A4-silenced cells compared with control cells (Figure 2A). However, removal of SCF for 16 h led to partial restoration of surface KIT expression in the MS4A4-silenced cells compared with control cells (Figure 2B). Subsequent induction of KIT internalization by exposing the SCF-deprived cells to 100 ng/ml SCF for 60 min demonstrated that control and MS4A4-silenced LAD-2 cells internalized KIT with similar efficacy (Figure 2C). Thus the greatest difference in surface expression of KIT between scrambled control and MS4A4-silenced cells was apparent when cells were continuously exposed to SCF, as shown in Figure 2, D and E ("no starving"). These data indicate that, in the presence of SCF, surface KIT expression is held in dynamic equilibrium between internalization and recycling of KIT to the cell surface, with either or both processes being retarded with MS4A4 silencing.

To assess the effect of MS4A4 silencing on KIT turnover, we undertook kinetic studies using flow cytometry. In the presence of 100 ng/ml SCF, KIT internalization followed a typical decay curve. Calculation of the half-life ($t_{1/2}$) of surface receptor expression by nonlinear regression indicated a $t_{1/2}$ of KIT internalization of 6.17 ± 0.85 min in control LAD-2 cells and 4.01 ± 0.42 min in MS4A4-silenced cells (Figure 2F; $n = 5$, $p = 0.025$, paired t test for $t_{1/2}$). Because loss of surface expression of receptors could involve changes in the rate of recycling as well as endocytosis of receptors, we also used a pulse-chase method that eliminates repeated cycling of receptors. By use of a previously published pulse-chase procedure (Roepstorff *et al.*, 2009), we found that although there was increased endocytosis of KIT with MS4A4 silencing (Figure 2F), there was no apparent recycling of KIT with 100 ng/ml SCF in either scramble control or shMS4A4-treated cells (Figure 2G). We also determined whether KIT was degraded more readily with MS4A4 silencing by using the pulse-chase method in the presence of cycloheximide (10 μM) and found no alteration in KIT degradation after stimulation with 100 ng/ml SCF when MS4A4 was silenced (Figure 2H).

Because trafficking of RTKs can depend on the concentration of ligand (Goh and Sorkin, 2013), we next studied the kinetics of KIT internalization with a lower concentration (10 ng/ml) of SCF. The rate and extent of KIT internalization were less with 10 ng/ml SCF (Figure 2I) than with 100 ng/ml SCF (Figure 2F), but the enhancement of KIT internalization with MS4A4 silencing was more pronounced at the lower concentration of SCF (Figure 2I). If high concentrations of ligand decrease efficiency of receptor recycling and increase degradation, this could account for the greater effect of MS4A4 silencing at the lower SCF concentration. To address this possibility, we examined KIT kinetics using the pulse-chase method with 10 ng/ml SCF. As expected and consistent with the internalization assays in the continuous presence of SCF (Figure 2, F and I), 10 ng/ml SCF resulted in less overall internalization than 100 ng/ml SCF (compare Figure 2, G and J). Silencing MS4A4 resulted in more rapid endocytosis, with maximal internalization evident at 5 min compared with 10 min in scramble control cells (Figure 2J). In addition, there was a consistent increase in surface expression of KIT at
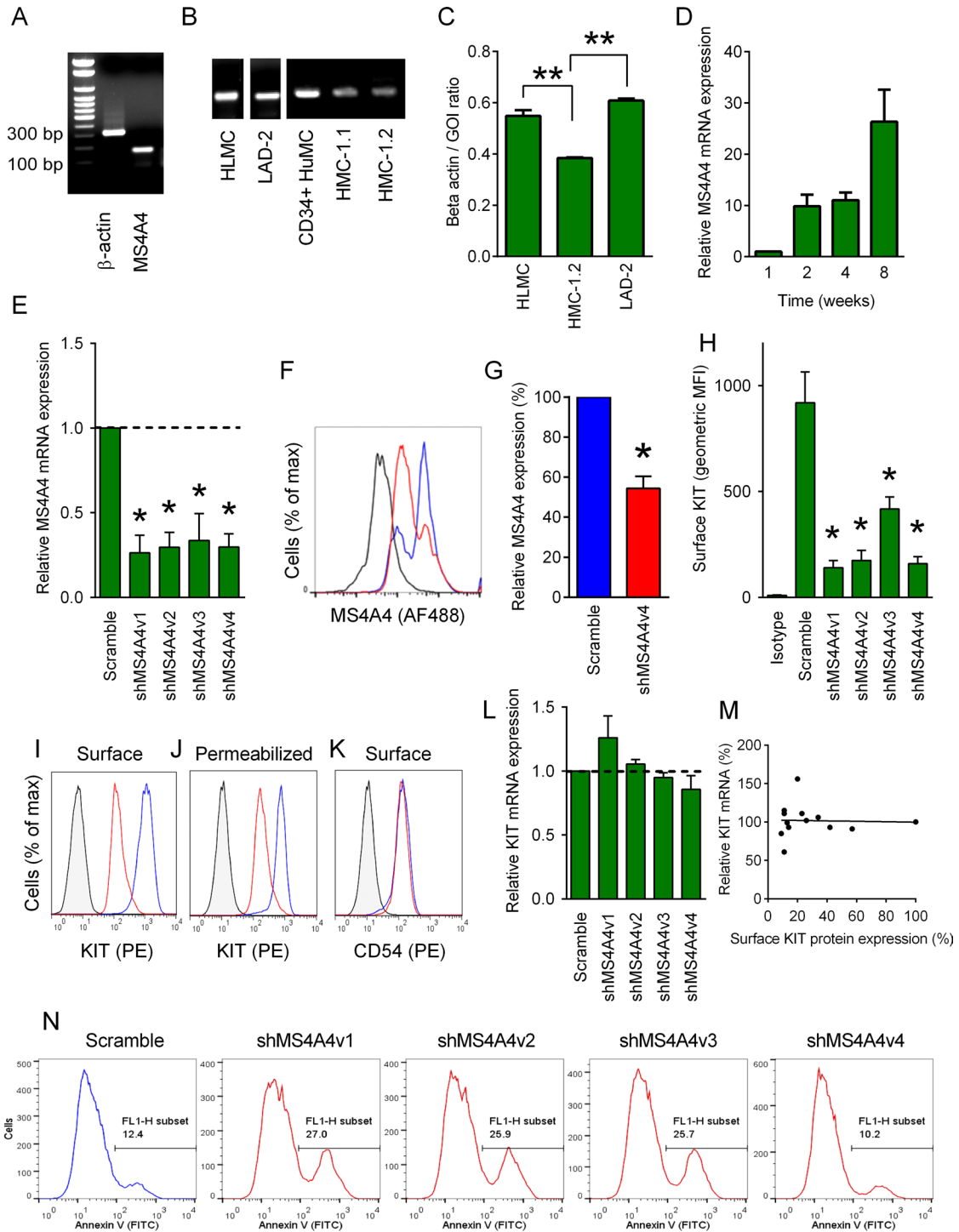
FIGURE 1: MS4A4 in human MC promotes surface KIT receptor expression. (A) RT-PCR for MS4A4 and β-actin in HLMCs. (B) All human MC types tested expressed MS4A4 mRNA. (C) qRT-PCR for MS4A4 mRNA in human MCs. Data calculated as the ratio of MS4A4 compared with β-actin for each sample ($n = 3–11$). (D) qRT-PCR for MS4A4 mRNA in CD34^{+}-derived peripheral blood MC over time during culture ($n = 3$). (E) qRT-PCR for MS4A4 mRNA in LAD-2 cells using four shRNA constructs targeting MS4A4 ($n = 5$). (F) Flow cytometry histogram of total MS4A4 protein expression in LAD-2 cells treated with scrambled shRNA control or the shMS4A4v4 construct (isotype, black; scramble, blue; shMS4A4v4, red). (G) Mean flow cytometry data for MS4A4 expression calculated from the geometric MFI and expressed as percentage of scramble control ($n = 4$). (H) Mean flow cytometry data for surface KIT expression in shMS4A4-transduced LAD-2 cells ($n = 4$). (I) Flow cytometry histogram of surface KIT expression. (J) Flow cytometry histogram of total KIT expression in permeabilized cells. (K) Flow cytometry histogram of surface CD54 expression. (L) qRT-PCR for KIT mRNA with shMS4A4 constructs. Values are relative expression compared with scramble control ($n = 3$). (M) Correlation between surface KIT protein expression and relative KIT mRNA expression calculated as relative percentage compared with scramble control. (N) Flow cytometry histograms of annexin V staining from LAD-2 cells transduced with either control shRNA or shMS4A4 constructs at day 7 postinfection. Data are mean + SEM. *$p < 0.05$, **$p < 0.001$.
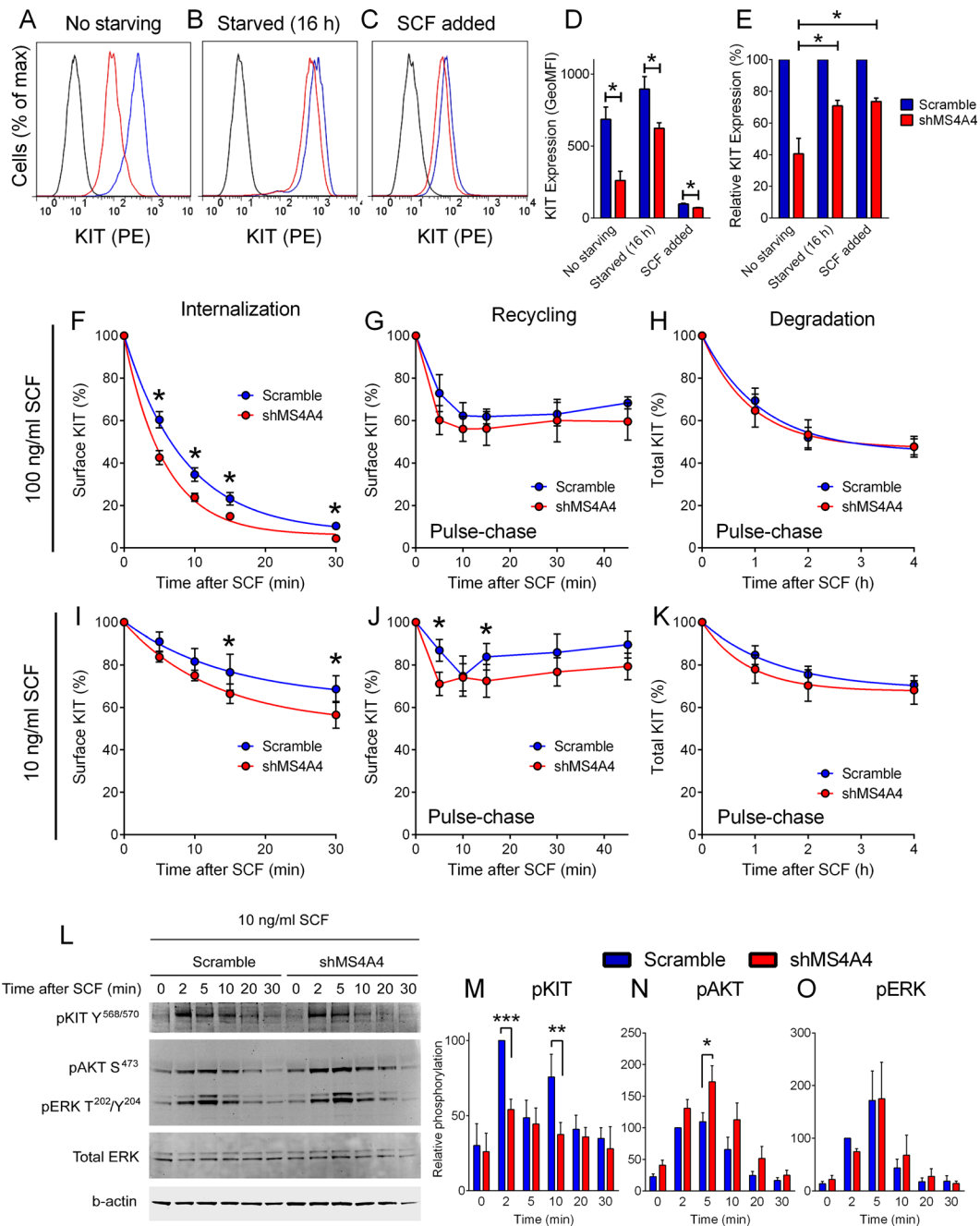
FIGURE 2: Silencing MS4A4 alters KIT internalization, recycling to the plasma membrane and signaling in LAD-2 cells. (A) Flow cytometry histogram showing surface KIT expression at day 7 postinfection with shMS4A4. (B) Flow cytometry histogram showing surface KIT expression after 16 h of SCF withdrawal. (C) As in B, but followed by stimulation with 100 ng/ml SCF for 1 h. Isotype, black; scramble, blue; shMS4A4, red). (D) Average flow cytometry data from SCF exposure experiments, Values are geometric mean fluorescence intensity (MFI; error bars, SEM; $n = 3$). (E) Average flow cytometry data calculated as percentage expression normalized to scramble control (error bars, SEM; $n = 3$). (F) Average flow cytometry data from KIT internalization assays after exposure to 100 ng/ml SCF. SCF was withdrawn for 16 h before experiment ($n = 5$, $p = 0.0008$, two-way ANOVA scramble vs. shMS4A4). *$p < 0.05$, Sidak's posttest. (G) KIT kinetics assay using SCF pulse chase with 100 ng/ml SCF. The x-axis is the time spent at 37°C during chase ($n = 3$). (H) KIT degradation assay using pulse chase with 100 ng/ml SCF in the presence of 10 μM cycloheximide and staining for surface and intracellular KIT. (I) As in F, after exposure to 10 ng/ml SCF. BFA was included to eliminate repopulation of surface KIT from newly synthesized pools ($n = 4$, $p = 0.047$, two-way ANOVA scramble vs. shMS4A4). *$p < 0.05$, Sidak's posttest. (J) KIT kinetics assay using pulse chase with 10 ng/ml SCF. The x-axis is the time spent at 37°C during chase ($n = 3$). *$p < 0.05$, Sidak's posttest. (K) KIT degradation assay by using pulse chase with 10 ng/ml SCF in the presence of 10 μM cycloheximide and staining for surface and intracellular KIT. (L) Immunoblots for pKIT Y[568/570] (Invitrogen antibody), pAKT S[473], and pERK T[202]Y[204] in scramble shRNA control and shMS4A4- treated LAD-2 cells for the indicated time after stimulation with 10 ng/ml SCF. (M) Analysis of fluorescence intensity (LI-COR system) of phosphorylated KIT (M), AKT (N), and ERK (O) after correction against loading control normalized to percentage of scramble control at 2 min (mean + SEM, $n = 5$). *$p < 0.05$, **$p < 0.01$, ***$p < 0.001$, ANOVA with Sidak's posttest.

15 min when compared with 10 min in control cells, which was not evident with MS4A4 silencing (Figure 2J). This increase in surface KIT expression most likely represents KIT recycling. Despite more rapid endocytosis and reduced recycling of KIT with MS4A4 silencing, there was no significant difference in KIT degradation with 10 ng/ml SCF (Figure 2K; $p = 0.3997$, two-way analysis of variance [ANOVA] scramble vs. shMS4A4, $n = 3$). These data are consistent with the conclusion that MS4A4 contributes to both stabilization of KIT at the cell surface and recycling and repopulation of KIT in the plasma membrane and thus regulates the steady-state dynamics of KIT at the cell surface.

KIT signaling is altered with MS4A4 silencing

We next examined whether the effects of MS4A4 silencing on KIT internalization altered MC signaling through KIT. An early signaling event in the KIT activation cascade in MCs is *trans*-phosphorylation of Tyr-568/570 residues of KIT (Blume-Jensen et al., 1991; Pawson, 2004; Ronnstrand, 2004) to initiate Src family kinase–mediated signaling pathways (Linnekin et al., 1997; Abram and Courtneidge, 2000). These events most likely occur at the plasma membrane within lipid raft microdomains (Kovarova et al., 2001; Arcaro et al., 2007; Jahn et al., 2007). SCF (100 ng/ml) induced rapid phosphorylation of KIT Tyr-568/570 in control LAD-2 cells, and such phosphorylation was reduced in MS4A4-silenced cells (Supplemental Figure S2). Paradoxically, later signaling events, including the activating phosphorylations of AKT (Ser-473) and ERK (Thr-202/Tyr-204), were not significantly different despite diminished expression and phosphorylation of KIT in MS4A4-treated cells (Supplemental Figure S2).

We also examined KIT-mediated signaling with 10 ng/ml SCF because the differences in kinetics of KIT internalization were more apparent at this concentration of SCF when analyzed by the pulse-chase procedure (Figure 2J). SCF at 10 ng/ml also induced rapid phosphorylation of KIT (Tyr-568/570) within 2 min, which was significantly reduced in shMS4A4-treated cells (Figure 2, L and M). A significant reduction in phosphorylation of KIT was also evident at 10 min with shMS4A4 treatment (Figure 2, L and M). Of interest, phosphorylation of KIT appeared to increase at 10 min when compared with 5 min in scramble control cells but not in MS4A4-silenced cells (Figure 2, L and M) and might be a consequence of KIT recycling. In contrast to reduced KIT phosphorylation, phosphorylation of AKT (Ser-473) was enhanced with MS4A4 silencing, which was particularly evident at 5 min (Figure 2, L and N). We did not detect any significant difference in ERK phosphorylation with shMS4A4 treatment (Figure 2, L and O). Taken together, these data indicate that silencing MS4A4 enhances AKT signaling despite reduced KIT phosphorylation.

MS4A4 colocalizes with KIT after SCF exposure

Because MS4A4 may facilitate KIT receptor surface expression by influencing both receptor internalization and receptor recycling pathways, we explored whether MS4A4 and KIT colocalized to the plasma membrane and intracellular organelles. We performed confocal microscopy on LAD-2 cells transfected with enhanced green fluorescent protein (EGFP)–tagged MS4A4 in both fixed and live cells after SCF stimulation. Transfected MS4A4 localized to a juxtanuclear region, as well as in distinct vesicles throughout the body and periphery of the cell, with evidence of some plasma membrane localization (Figure 3A), although this localization was somewhat variable among cells. MS4A4 exhibited low colocalization with endogenous KIT in the absence of SCF, which was observed in both vesicles and the plasma membrane (Figure 3A). However, after

exposure to SCF, MS4A4 and KIT colocalized to intracellular vesicles, especially in the centrosomal region (Figure 3, A and B). Particularly striking was the widespread intracellular distribution of KIT in the absence of SCF stimulation, which may be indicative of continuous turnover of KIT in nonstimulated LAD-2 cells.

We next determined whether the intracellular structures associated with MS4A4 were early endosomes (EEs). Transfection of MS4A4 into LAD-2 cells displayed some localization, which appeared to be the endoplasmic reticulum (Figure 3C). Indeed, cotransfection of MS4A4 and Sec61B (a marker of the endoplasmic reticulum) in HEK293T cells demonstrated a degree of colocalization in some cells (Supplemental Figure S3A). We therefore performed immunofluorescence (IF) for endogenous MS4A4 using a mouse polyclonal antibody (Ab) and found that the distribution of native MS4A4 was comparable to that of overexpressed MS4A4, except that native MS4A4 displayed a more punctate morphology (Figure 3C). We confirmed that anti-MS4A4 was immunoreactive to MS4A4 by performing IF on MS4A4-transfected HEK293T cells (Supplemental Figure S3, B–D). Having validated Ab specificity, we performed IF on LAD-2 cells costained with the EE marker EEA1 and determined that MS4A4 and EEA1 colocalized to early endosomes surrounding an MS4A4$^+$ juxtanuclear compartment (Figure 3D). The colocalization of MS4A4 and EEA1 was significantly decreased after 5 min of stimulation with SCF, although this decrease was no longer significant at later time points (Figure 3E). The relevance of this decreased colocalization at early time points after SCF stimulation is not clear but could be due to rapid MS4A4 cycling to the plasma membrane in response to SCF. However, more study is required to determine whether this observation is relevant to the function of MS4A4.

MS4A4 colocalizes with Rab5 in endosomes

The concerted action of Rab family proteins and their effector proteins regulates almost all membrane and protein trafficking in eukaryotic cells (Mizuno-Yamasaki et al., 2012). An important component of endocytic trafficking and recycling pathways is Rab5, which is a key regulator of early endocytic events and the sorting endosome (Woodman, 2000; Stenmark, 2009) and participates in receptor trafficking in mast cells (Kalesnikoff et al., 2007; Rios et al., 2008; Kageyama-Yahara et al., 2011). Rab5 facilitates vesicle fusion and is critical for the formation of EEs by fusion of endocytic vesicles (for review, see Woodman, 2000). Thus constitutively active Rab5 (Q79L) promotes enlarged EE formation, whereas dominant-negative Rab5 (S34N) perturbs endocytic vesicle fusion and endosomal formation (Stenmark et al., 1994).

Because MS4A4 appeared to traffic through the endocytic system, the passage of MS4A4 through Rab protein–regulated endocytic trafficking pathways was examined by cotransfection of fluorescent protein–tagged MS4A4 and various Rab proteins and their variants in live LAD-2 cells. With respect to Rab5, there was substantial colocalization of MS4A4 in enlarged endosomes (up to 2 μm in diameter) with both wild-type Rab5 (Figure 4A, left) and constitutively active Rab5 (Q79L; Figure 4A, middle). However, cotransfection of MS4A4 with constitutively active Rab5 (Q79L) led to formation of very large endosomes (>4 μm in diameter), most of which were not positive for MS4A4 (Figure 4A, middle). Consequently colocalization of MS4A4 with constitutively active Rab5 decreased compared with wild-type Rab5 (Figure 4B). This observation may be related to the decrease in colocalization between MS4A4 and EEA1 in response to SCF (Figure 3E). MS4A4 localization to enlarged early endosomes was dependent on active Rab5 since cotransfection of dominant-negative Rab5 (S34N) and MS4A4 showed no evidence
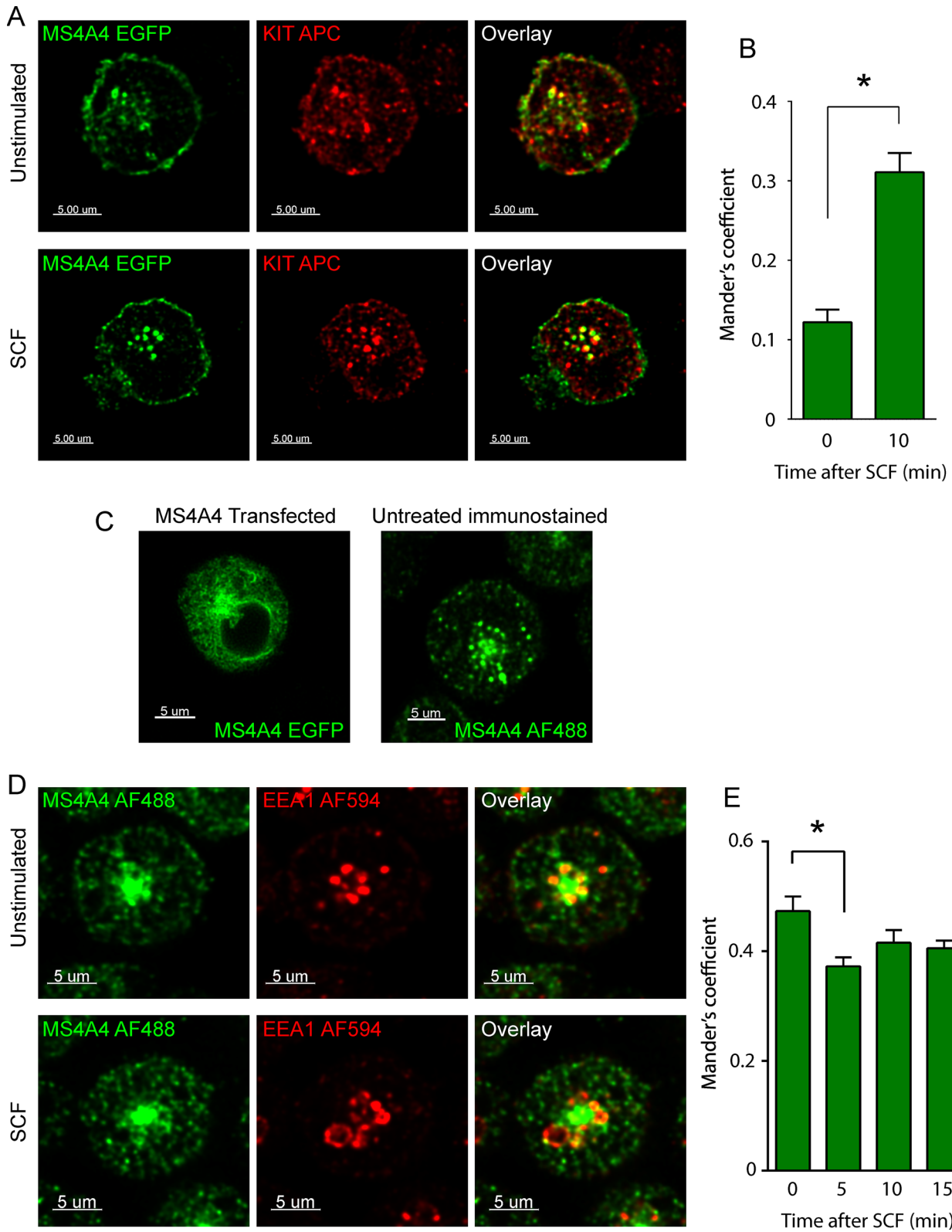
FIGURE 3: MS4A4 colocalizes with KIT and EEA1 in LAD-2 cells. (A) Confocal micrographs of LAD-2 cells transfected with MS4A4:EGFP chimeric protein (green) immunostained for KIT (APC) (red) in the absence (top) or after stimulation with SCF (bottom). (B) Manders coefficient of colocalization for MS4A4 and KIT. (C) Confocal micrographs of LAD-2 cells transfected with MS4A4:EGFP (left) or cells immunostained with anti-MS4A4 followed by AF488-labeled anti-mouse secondary (right). (D) Immunofluorescence confocal micrographs of LAD-2 cells immunostained for mouse anti-MS4A4 (secondary, AF488) and rabbit anti-EEA1 (secondary, AF594) in the absence of SCF (top) or with SCF stimulation for 10 min (bottom). Scale bars, 5 μm. (E) Manders coefficient of colocalization for MS4A4 and EEA1. For B and E, bars are the mean + SEM from the volume of 16 stacks of images from two separate experiments). *$p < 0.05$, ANOVA with Sidak's posttest.
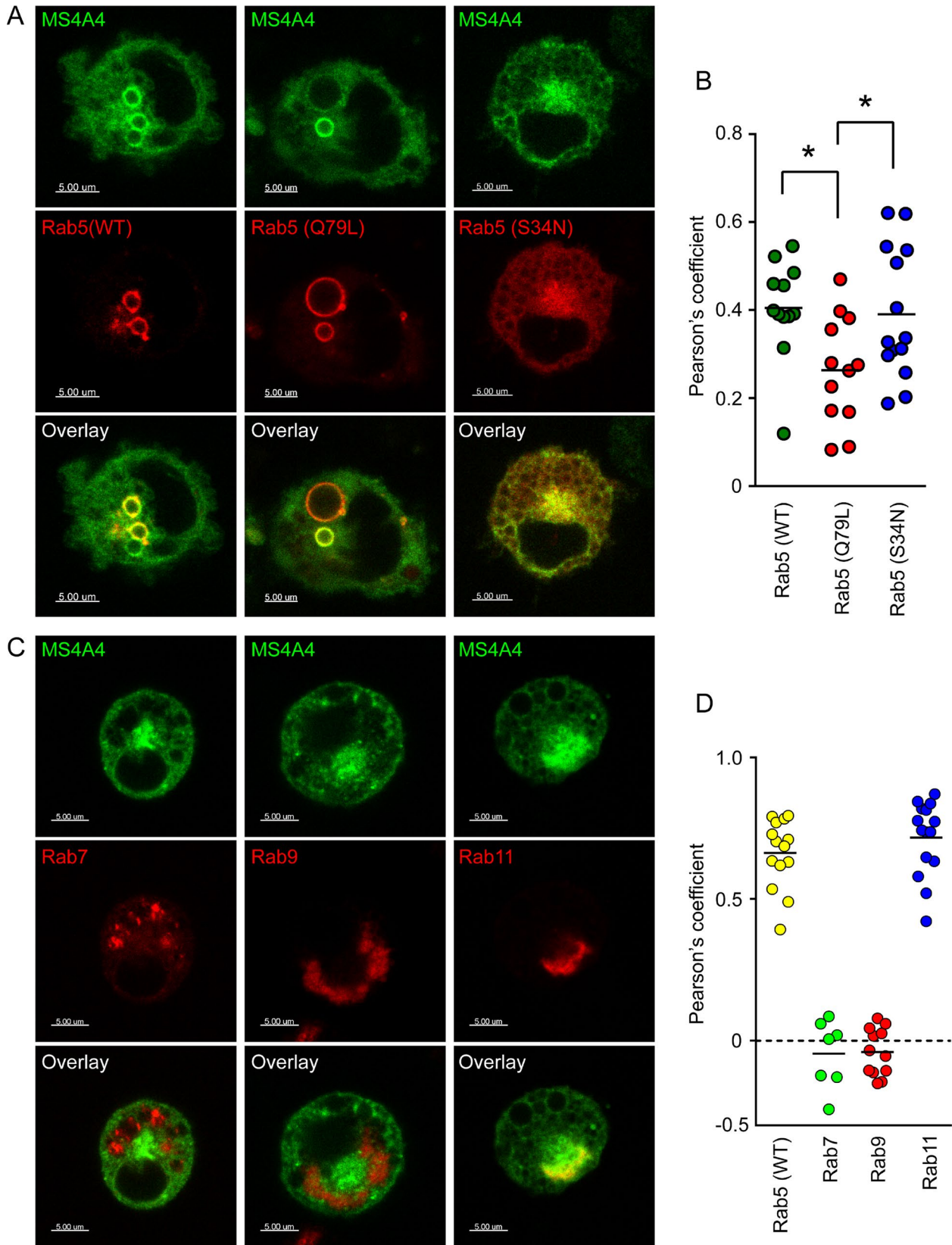
FIGURE 4: MS4A4 traffics through endocytic recycling pathways. (A) Confocal micrographs of live LAD-2 cells cotransfected with MS4A4:EGFP and mRFP Rab5 (left), constitutively active mCherry Rab5 (Q79L; middle), or dominant-negative mCherry Rab5 (S34N; right). (B) Pearson's coefficient in colocalized volumes of MS4A4 with wild-type Rab5, constitutively active Rab5, and dominant-negative Rab5. *$p < 0.05$. (C) Confocal micrographs of live LAD-2 cells cotransfected with MS4A4:EGFP and DsRed Rab7 (left), DsRed Rab9 (middle), or DsRed Rab11 (right). Scale bars, 5µm. (D) Pearson's coefficient in colocalized volumes of MS4A4 with Rab5, Rab7, Rab9, or Rab11.

of distinct endosomes. Instead, fluorescence for Rab5 (S34N) was more diffuse, and both MS4A4 and Rab5 (S34N) displayed some localization to a juxtanuclear region of the cell (Figure 4A, right). This distribution of MS4A4 with cotransfection of dominant-negative Rab5 (S34N) resembled the distribution of single transfection of MS4A4 into LAD-2 cells (compare Figure 4A to Figure 3B). Cotransfection of MS4A4 and Rab5 variants in HEK293T cells, which do not express KIT, exhibited limited colocalization of MS4A4 and WT Rab5 (Supplemental Figure S4A). However, cotransfection of MS4A4 and the constitutively active Rab5 (Q79L) showed marked colocalization (Supplemental Figure S4B). Therefore the pattern of MS4A4 colocalization with Rab5 variants in MC may differ from that of HEK293T cells, which do not natively express MS4A4 or KIT and are not dependent on growth factors for survival. Collectively these data indicate that MS4A4 trafficking in the endosomal compartments, but not colocalization with Rab5, appears to be dependent on active Rab5. In addition, when dominant-negative Rab5 (S34N) was transfected into LAD-2 cells, KIT no longer translocated to EEA1-positive EEs after stimulation with SCF, and staining of both KIT and EEA1 was diffuse (Supplemental Figure S5).

MS4A4 colocalizes with components of EEs and recycling compartments but not late endosomes in MCs

Because MS4A4 traffics with active Rab5 and colocalizes with KIT in EEs, we next examined the association of MS4A4 with other compartments of the endocytic pathways. Cargo that is not directed through recycling pathways remains in EEs and, during maturation into late endosomes (LEs), regulation switches from Rab5- to Rab7-mediated events such as lysosomal fusion and subsequently protein degradation (Poteryaev et al., 2010; Huotari and Helenius, 2011). Thus Rab7 localizes to LE and lysosomes. Using cotransfection of MS4A4 and Rab7 in LAD-2 cells, we determined that MS4A4 did not colocalize with Rab7 under any condition (Figure 4, C and D). Similarly, Rab9, which is also a LE marker and may regulate endosomes to trans-Golgi network trafficking of certain cargo (Stenmark, 2009), also localized to different cellular compartments than MS4A4 (Figure 4, C and D).

Because MS4A4 does not apparently migrate to LE compartments, we examined whether MS4A4 migrated instead to the endocytic recycling compartment (ERC), where Rab11 mediates receptor recycling back to the plasma membrane (Maxfield and McGraw, 2004; Grant and Donaldson, 2009). MS4A4 and Rab11 colocalized in LAD-2 cells within a juxtanuclear region. possibly indicative of an MS4A4+/Rab11+ compartment (Figure 4, C and D). In total, our cotransfection data demonstrate that MS4A4 localizes to components of EE pathways and the recycling pathway rather than the LE and degradation pathways.

Gene silencing of MS4A4 results in altered KIT trafficking and enlarged EEs

On the basis of the foregoing experiments, we hypothesized that MS4A4 promotes trafficking of KIT toward the ERC from EEs and that this results in reduced KIT degradation and greater steady-state KIT expression at the plasma membrane. This was tested by silencing of MS4A4 with shMS4A4, or scrambled shRNA as controls, in LAD-2 cells. We found that KIT was recruited to EEA1-positive EEs after stimulation with SCF in both control and MS4A4-silenced cells (Figure 5, A and B). However, KIT colocalizations with Rab5 and EEA1 were both reduced with gene silencing of MS4A4 (Figure 5, C and D), whereas colocalization of KIT with Rab9+ LEs was increased (Figure 5E). In addition, EEA1+ EEs were significantly larger in the MS4A4-silenced cells, compared with the control cells, after SCF

stimulation ($p < 0.0001$, ANOVA; Figure 5, B and F). A plausible explanation for enlarged EEs is that the EE burden is increased in the absence of MS4A4 because of more rapid endocytosis and reduced recycling. The reduction in KIT recycling may also promote more rapid transit of KIT into the late endosomal/endolysosomal compartments, where it has been reported that oncogenic KIT can signal through AKT pathways (Obata et al., 2014).

MS4A4 expression affects KIT internalization pathways and PLCγ1 phosphorylation

RTKs are internalized by both clathrin-mediated and clathrin-independent endocytosis (reviewed in Goh and Sorkin, 2013). We found that SCF stimulated increased colocalization of KIT with clathrin, but this increase was unaffected by silencing MS4A4 over the time course tested (10 min; Figure 6, A and B). However, the SCF stimulated increase in colocalization of KIT with the lipid raft protein caveolin-1 (Lajoie and Nabi, 2010) was reduced (Figure 6, C and D). We therefore examined whether MS4A4 itself colocalized with caveolin-1, especially since the mouse homologue of MS4A4, Ms4a4b, is recruited to lipid rafts after T-cell activation (Xu et al., 2006). Stimulation with SCF did not significantly affect MS4A4 and clathrin colocalization (Figure 7, A and B). However, MS4A4 and caveolin-1 colocalization rapidly increased with stimulation using SCF (Figure 7, C and D), suggesting that MS4A4 was recruited along with KIT to lipid raft microdomains in human LAD-2 cells.

We next investigated MS4A4 regulation of lipid raft–associated signaling events, in particular PLCγ1, for several reasons. As noted earlier, shMS4A4 reduces phosphorylation of KIT Y568/570 (Figure 2I), and this phosphorylation is critical for recruitment of SH2 domain–containing proteins such as Lyn and PLCγ1 by KIT (van der Geer et al., 1994; Linnekin et al., 1997; Abram and Courtneidge, 2000; Pawson, 2004; Ronnstrand, 2004). KIT signaling through Lyn kinase is promoted by lipid rafts (Arcaro et al., 2007; Jahn et al., 2007). In addition, we found that MS4A4 not only colocalized (Figure 7C) but also coimmunoprecipitated with caveolin-1 (Figure 7E). On examining PLCγ1 activation, we found that silencing MS4A4 blunted the phosphorylation of PLCγ1 (Figure 7, F and G). These data are compatible with our thesis that MS4A4 promotes recruitment of KIT to lipid raft microdomains, altering signaling and internalization pathways.

Silencing MS4A4 affects SCF-driven mast cell functional responses

We next examined the effects of MS4A4 silencing on SCF-mediated responses in MCs, given that MS4A4 can regulate KIT trafficking and recycling and that SCF is critical for MC growth, survival, differentiation, and migration. With respect to MC growth, we found that LAD-2 cell proliferation was enhanced with MS4A4 silencing, as demonstrated by an increase in viable cell number at 7 d (Figure 8A). SCF is a chemoattractant for MCs and thereby contributes to MC recruitment, survival, and proliferation in tissue (Okayama and Kawakami, 2006; Jensen et al., 2007; Halova et al., 2012). Because LAD-2 cells do not migrate well using standard chemotaxis assays, assays were performed instead as described (Cruse et al., 2006, 2011) with primary human CD34+ peripheral blood–derived MCs, which migrate well in response to SCF (Smrž et al., 2013). Silencing of MS4A4 significantly increased CD34+ MC migration to SCF when compared with scramble control cells (Figure 8B). Therefore the alteration in KIT trafficking and signaling on knockdown of MS4A4 is associated with increased SCF-driven responses such as MC migration and proliferation, as summarized schematically in Figure 8C.

DISCUSSION

In this study, we report that MS4A4 aids trafficking of the growth factor receptor tyrosine kinase KIT to the plasma membrane and maximizes expression of the receptor at the cell surface by promoting its recruitment to caveolin-1–enriched lipid rafts and directing internalized receptors toward the endocytic recycling pathway and away from LE and the degradation pathway. We propose that MS4A4 accomplishes this by directing a proportion of the receptors toward clathrin-independent endocytosis pathways and away from clathrin-mediated endocytosis pathways. There is growing evidence that mechanisms of internalization can alter the trafficking of endocytosed receptors by directing them toward either degradation or recycling pathways (Sigismund et al., 2008; Grant and Donaldson, 2009; Parachoniak et al., 2011) and that endocytic receptor trafficking and signal transduction are interrelated (Teis et al., 2002; Taub et al., 2007; Scita and Di Fiore, 2010; Platta and Stenmark, 2011; Brankatschk et al., 2012; Palfy et al., 2012). We demonstrate accordingly that MS4A4 alters KIT-mediated signaling through recruitment of KIT to lipid rafts and signaling through AKT and PLCγ1 pathways.

Growth factor receptors generate signals not only at the plasma membrane but also within intracellular organelles after endocytosis. The RTK epidermal growth factor receptor (EGFR), when activated at the plasma membrane, requires internalization into endosomal compartments for full activation of ERK (Vieira et al., 1996; Kranenburg et al., 1999). ERK signaling has been shown to occur in EEs (Hu et al., 2009; Brankatschk et al., 2012; Wu et al., 2012) and persists through endosomal maturation to LEs until passage into the lumen of lysosomes leads to cessation of signaling (Burke et al., 2001). The present study shows that silencing MS4A4 does not affect global ERK signaling but does affect KIT trafficking by increasing endocytosis and reducing KIT recycling, which may promote KIT transit into LEs. However, the possibility remains that the location of ERK signaling within the cell may be altered by the changes in KIT trafficking.

Another factor governing signal transduction and functional outcomes is that the composition of scaffold complexes and adaptor proteins may vary from one subcellular compartment to another and thus determine spatiotemporal characteristics of signal transduction (Kolch, 2000; Teis et al., 2002; Taub et al., 2007). In particular, ERK signal transduction initiated by the EGFR is dependent on LE localization of MEK1 partner (MP1) and p14 proteins (Teis et al., 2002), and disruption of p14-MP1-MEK1 endosomal signaling inhibits proliferation (Teis et al., 2006).

The aforementioned studies suggest that in addition to signaling at the plasma membrane, intracellular localization of receptors may affect growth factor–dependent proliferation. Indeed, hematopoietic cell transformation by activating mutations in RTKs exhibit intracellular localization of receptors, which appears to be critical for the proliferative response (reviewed by Toffalini and Demoulin, 2010). A specific example is that neoplasia associated with activating mutations in KIT is driven by intracellular and perinuclear signaling rather than plasma membrane signaling (Xiang et al., 2007). How signaling may be dependent on the intracellular localization of RTKs has also been shown using the hepatocyte growth factor receptor (c-MET), which is unable to activate the transcription factor STAT3 at the plasma membrane but can trigger nuclear accumulation of STAT3 when activated from endosomal compartments (Kermorgant and Parker, 2008). Conversely, endocytosis may limit particular signaling pathways that require substrates found in the plasma membrane. For example, PLCγ1 and phosphatidylinositol-3-kinases (PI3Ks) use phosphatidylin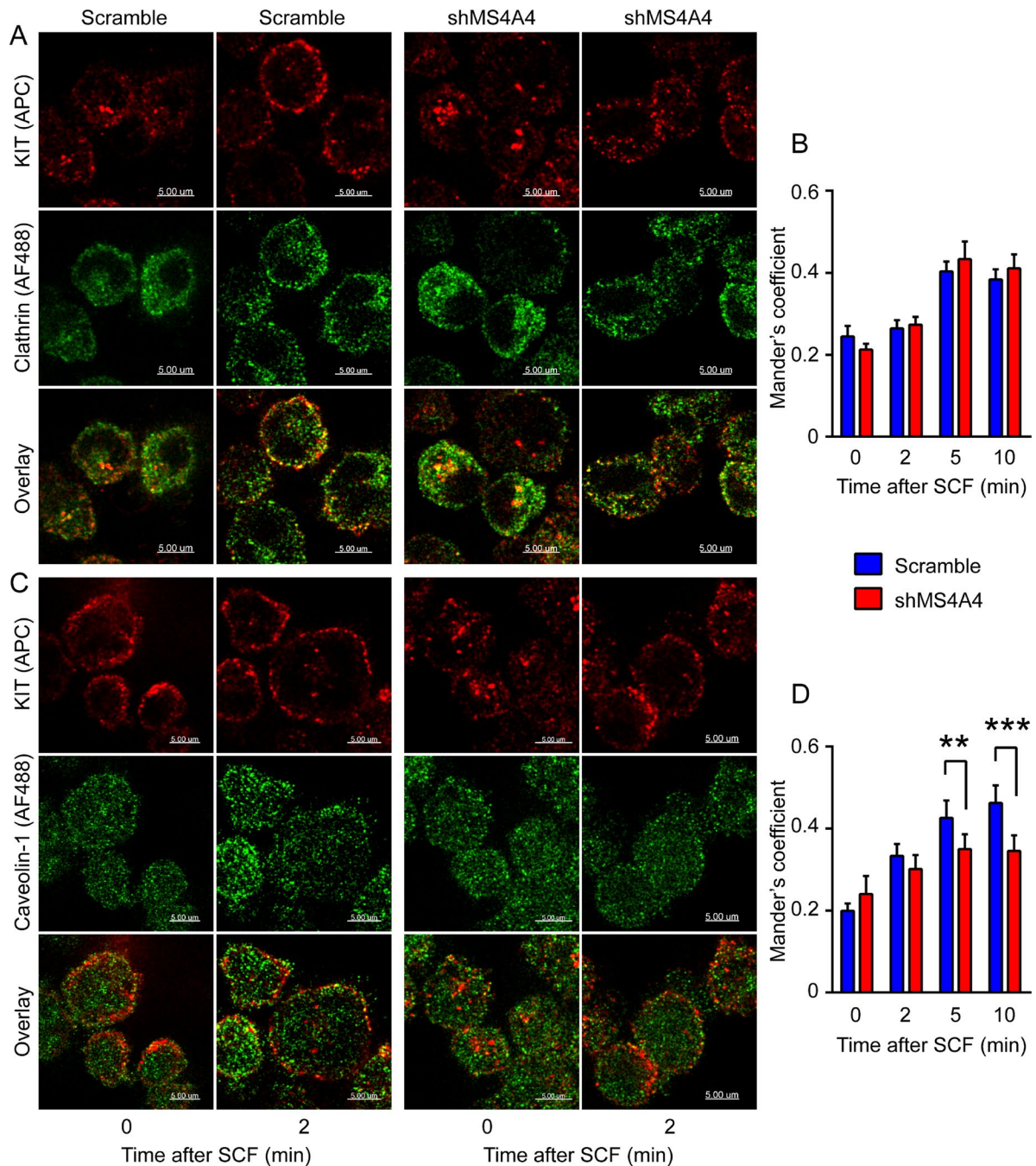ositol-4,5-biphosphate as substrate within the plasma membrane, whereas their access to this substrate is limited in endosomes (Haugh and Meyer, 2002). Therefore the promotion of plasma membrane signaling by up-regulation of MS4A4 may alter the functional outcome of SCF signals because PI3K signaling appears to be critical for MC maturation (Ma et al., 2011).

Other indications that cellular localization of KIT determines signaling and functional outputs include the observation that altered trafficking of KIT in bone marrow–derived MC (BMMC) by targeting small ARF GTPase-activating protein 1 (SMAP1) led to intracellular retention of KIT and hyperphosphorylation of ERK, which may predispose mice to myelodysplasia and acute myeloid leukemia (Kon et al., 2013). The mechanism for endosomal KIT retention in SMAP1$^{-/-}$ BMMCs is distinct from that of MS4A4 silencing. The attendant changes in signaling also appear to be different, since silencing of MS4A4 promoted AKT rather than ERK signaling. However, the functional consequences may be similar, as the PI3K/AKT pathway is a well-established pathway in malignant lymphocytes (Blachly and Baiocchi. 2014). In addition, neoplastic KIT has been reported to be endocytosed via clathrin-mediated endocytosis and to signal through AKT pathways in endolysosomes, which is critical for proliferation (Obata et al., 2014). MS4A4 and SMAP1 both participate in KIT trafficking but in different endosomal compartments, with MS4A4 promoting KIT trafficking from the early sorting endosome to the plasma membrane (present study) and SMAP1 promoting KIT trafficking from LEs to lysosomes (Kon et al., 2013). However, disruption of either MS4A4 or SMAP1 leads to dysregulated KIT trafficking and signaling. Our data might also imply that MS4A4 promotes MC KIT-mediated differentiation and maturation because MS4A4 is preferentially expressed in mature MCs and a relatively mature secretory and slowly dividing MC line (LAD-2) as compared with an immature nonsecretory and proliferative MC line (HMC-1). Indeed, silencing MS4A4 promoted proliferation and migration of MCs in response to SCF, and thus these cells may represent a more immature phenotype. Moreover, MS4A4 mRNA expression increased substantially with maturation of HuMC cultures from CD34$^+$ progenitors during 8 wk of culture (Figure 1D).

It has also been suggested that MS4A4 may promote immune cell survival because silencing of the mouse homologue, Ms4a4b, induces mouse T-cell apoptosis (Yan et al., 2013). In addition, injection of antibodies to Ms4a4b into mice ameliorates experimental autoimmune encephalomyelitis by inducing apoptosis of activated T-cells accompanied by decreased Th1- and Th17-cell responses (Yan et al., 2013). Three of the shRNA constructs we tested induced MC apoptosis by 7 d posttransduction (Figure 1N). We selected a fourth shRNA construct and dose that did not induce apoptosis over the time course of the experiments to enable determination of the role of MS4A4 on KIT trafficking in healthy cells. This construct also induced apoptosis at later time points or higher doses, but under the nonapoptotic conditions used here, we could achieve ~50% reduction in MS4A4 protein expression (Figure 1G), which was sufficient to observe differences in KIT trafficking and actually promoted proliferation. Therefore MS4A4 expression may inversely correlate with MC proliferation, but low-level expression appears to be required for MC survival, since human MCs have an absolute requirement for SCF to prevent apoptosis (Okayama and Kawakami, 2006; Jensen et al., 2007), and thus loss of MS4A4 expression could also result in loss of KIT expression.

In agreement with our data in human MCs, the mouse homologue, Ms4a4b, enhances signaling through the T-cell glucocorticoid-induced tumor necrosis factor receptor GITR (Howie et al., 2009) and the TCR immunoreceptor (Xu et al., 2006) and is recruited to lipid rafts after T-cell stimulation (Xu et al., 2006). Taken together,

FIGURE 5: Silencing MS4A4 alters endocytic KIT trafficking. (A) Immunofluorescence confocal microscopy of scramble shRNA–treated (top) and shMS4A4-treated (bottom) LAD-2 cells stained with rabbit anti-EEA1 (secondary AF488; green) and mouse anti-KIT (APC; red) in the absence of SCF. White arrowhead shows occasional enlarged endosomes in shMS4A4-treated cells. Right, superimposed z-projection of the stack of images. Scale bars,

FIGURE 6: Silencing MS4A4 alters KIT colocalization with caveolin-1 but not clathrin. (A) Immunofluorescence confocal microscopy of scramble shRNA–treated (left) and shMS4A4- treated (right) LAD-2 cells stained with rabbit anti-clathrin HC (secondary, AF488; green) and mouse anti-KIT (APC, red) left unstimulated or stimulated with SCF for 2 min. Scale bars, 5 μm. (B) Manders coefficient of colocalization of KIT and clathrin HC at times indicated (minutes) after SCF stimulation. (C) Immunofluorescence confocal microscopy of scramble shRNA–treated (left) and shMS4A4-treated (right) LAD-2 cells stained with rabbit anti–caveolin-1 (secondary, AF488; green) and mouse anti-KIT (APC, red) left unstimulated or stimulated with SCF for 2 min. Scale bars, 5 μm. (D) Manders coefficient of colocalization of KIT and caveolin-1 with SCF stimulation time course. For B and D, bars are mean + SEM from the volume of 16 stacks of images from two separate experiments. **$p < 0.01$, ***$p < 0.001$, two-way ANOVA.

10 μm. (B) Immunofluorescence confocal microscopy after stimulation with SCF for 10 min. Yellow arrowheads show enlarged endosomes positive for KIT. Orange arrowheads show very large endosomes in shMS4A4-treated cells that are negative for KIT immunofluorescence. Scale bars, 10 μm. (C–E). Manders coefficient of colocalization of KIT and Rab5 (C), KIT and EEA1 (D), and KIT and Rab9 (E) before and after stimulation with SCF. Scramble shRNA, blue bars; shMS4A4, red bars. (Bars are mean + SEM from the volume of 16 stacks of images from two separate experiments.) (F). Endosome size from the volume of image stacks calculated using Imaris software. Two observers obtained comparable measurements. Scramble shRNA, blue circles; shMS4A4, red circles. For C–F, *$p < 0.05$, **$p < 0.01$, ***$p < 0.001$, two-way ANOVA.
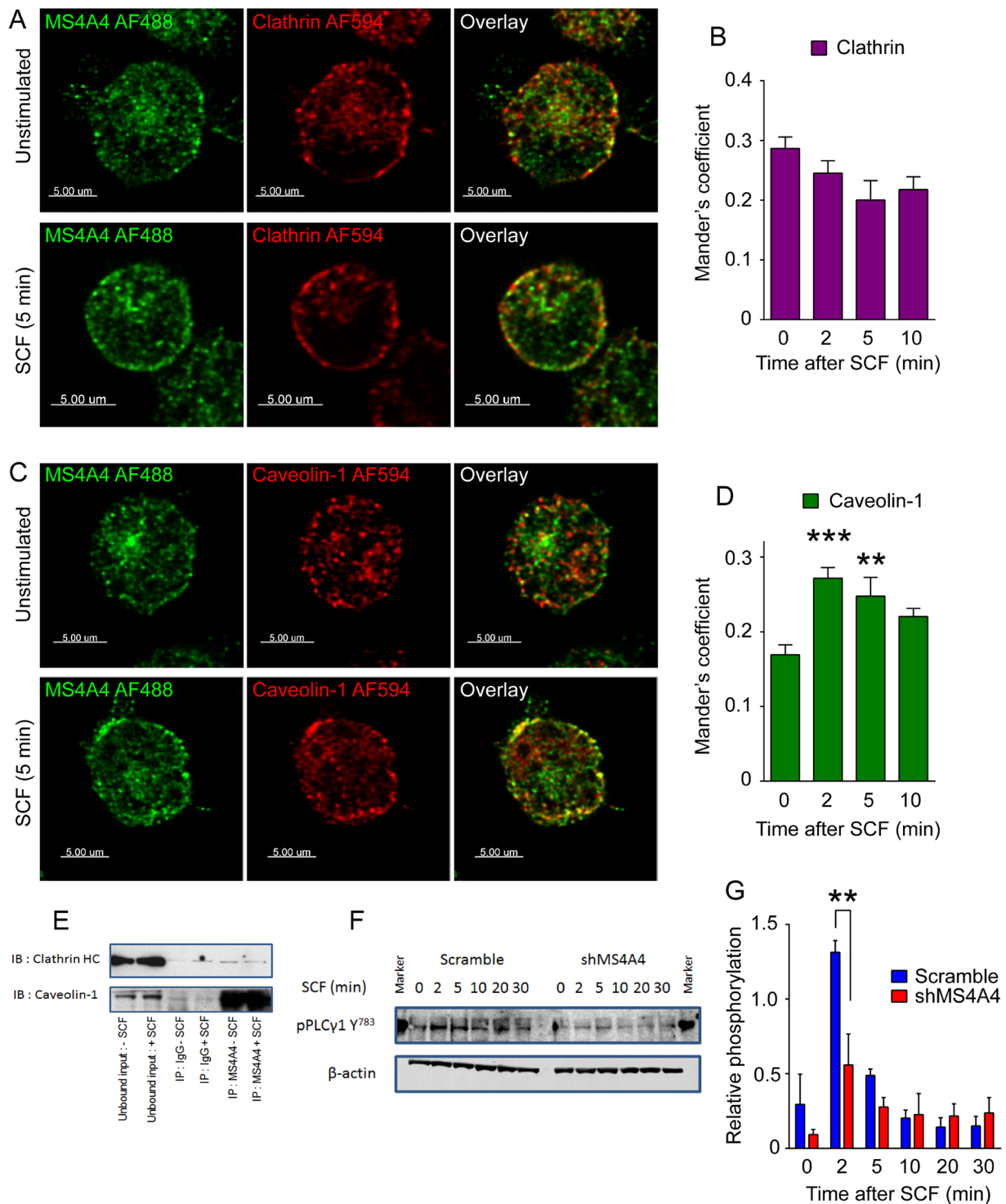
FIGURE 7: MS4A4 colocalizes preferentially with caveolin-1 over clathrin after stimulation with SCF promoting PLCγ1 phosphorylation. (A) LAD-2 human mast cells immunostained with mouse anti-MS4A4 and rabbit anti-clathrin HC, followed by anti-mouse AF488 and anti-rabbit AF594 before (top) and after SCF stimulation (bottom). No increase in colocalization was observed with stimulation. (B) Manders coefficient of colocalization of MS4A4 and clathrin HC with SCF stimulation time course. (C) LAD-2 human mast cells immunostained with mouse anti-MS4A4 and rabbit anti–caveolin-1 demonstrated an increase in colocalization with SCF stimulation (bottom) compared with untreated cells (top). Scale bars, 5 μm (A, C). (D) Manders coefficient of colocalization of MS4A4 and caveolin-1 with SCF stimulation time course. For B and D, bars are the mean + SEM from the volume of 15 stacks of images from two separate experiments. **$p < 0.01$, ***$p < 0.001$, two-way ANOVA. (E) Coimmunoprecipitation using anti-MS4A4 or IgG control as pull down. Immunoblots for clathrin HC and caveolin-1. (F) Immunoblot of PLCγ1 Y783 phosphorylation in response to SCF stimulation over time. β-Actin was used as a control. (G) Densitometry of phosphorylated PLCγ1 (Y783) after correction. Average data from three experiments. Error bars, SEM. **$p < 0.01$.
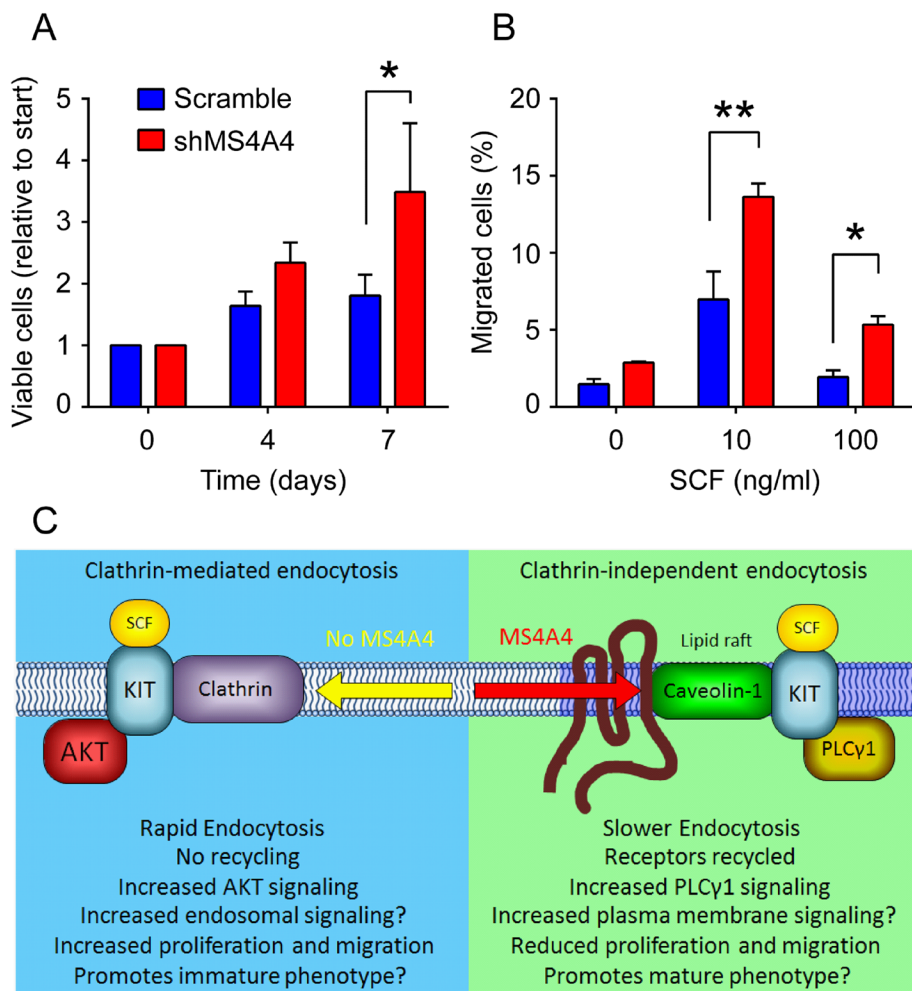
FIGURE 8: Silencing MS4A4 promotes mast cell proliferation and migration. (A) LAD-2 human mast cells treated with scramble shRNA or shMS4A4 were cultured under normal conditions and counted at the indicated time points using flow cytometry. Cell counts are presented as viable cells relative to starting number. (B) CD34+ peripheral blood–derived mast cell migration was assessed using a Transwell system. Bars are the mean + SEM from three experiments. *$p < 0.05$, **$p < 0.01$. (C) Schematic summary of proposed function for MS4A4. MS4A4 directs recruitment of KIT to caveolae, altering trafficking, signaling, and function of KIT.

these observations suggest that MS4A4 function is not restricted to any one receptor but may have corresponding functions with other receptors.

In summary, this study identifies a novel function for MS4A4 in that it aids trafficking of KIT to the plasma membrane and promotes lipid raft–associated PLCγ1 signaling pathways while reducing AKT signaling. We propose that MS4A4-mediated KIT trafficking to lipid raft microdomains at the plasma membrane regulates KIT signaling and downstream endocytic trafficking (summarized in Figure 8C). We believe that this study sheds new light on the mechanism of action of many MS4A family proteins, highlighting their potential as therapeutic targets. An excellent example of targeting the MS4A family already exists with the efficacy of rituximab (anti-MS4A1) for treating non–Hodgkin's B-cell lymphoma. In addition, anti-Ms4a4b antibodies injected into mice induces apoptosis of activated T-cells and ameliorates experimental autoimmune encephalomyelitis (Yan et al., 2013). Given the function of MS4A4 as reported here, MS4A4 may provide an additional target for modulating the progression of MC-dependent diseases and possibly other immune diseases.

MATERIALS AND METHODS

Antibodies

The following antibodies were purchased: phycoerythrin (PE)-conjugated mouse anti-CD117 (clone 104D2; Biolegend, San Diego, CA), allophycocyanin (APC)-conjugated mouse anti-CD117 (BD PharMingen, San Jose, CA), PE-conjugated mouse anti-CD54 (BD PharMingen), mouse anti–β-actin (clone AC-15; Sigma-Aldrich, St. Louis, MO), AF647-conjugated mouse anti-GM130 (clone 35/GM130; BD PharMingen), mouse polyclonal anti-MS4A4 (Sigma-Aldrich), rabbit anti-EEA1 (Cell Signaling, Danvers, MA), rabbit anti-Rab5 (Cell Signaling), rabbit anti-Rab9 (clone D52G8; Cell Signaling), rabbit anti–clathrin heavy chain (P1663; Cell Signaling), and rabbit anti–caveolin-1 (Cell Signaling). The following phosphorylation-specific antibodies were purchased: rabbit anti-pPLCγ1 (Tyr-783), rabbit anti-pAkt (Ser-473), and rabbit anti-pERK1/2 (Thr-202/Tyr-204; all from Cell Signaling) and rabbit anti-pKIT (Tyr-568/570; Biosource, Carlsbad, CA), rabbit anti-pKIT (Tyr-568/570; Invitrogen, Carlsbad, CA), and rabbit anti-pPLCγ1 (Tyr-783; Biosource). The secondary antibodies horseradish peroxidase (HRP)–conjugated rabbit anti-goat immunoglobulin G (IgG), HRP-conjugated goat anti-rabbit IgG, and HRP-conjugated goat anti-mouse IgG (Santa Cruz Biotechnology, Dallas, TX) and Alexa Fluor–conjugated goat anti-mouse AF488, goat anti-mouse AF568, goat anti-mouse AF594, goat anti-rabbit AF405, goat anti-rabbit AF488, and goat anti-rabbit AF594 (Invitrogen) were purchased.

Human mast cell culture

LAD-2 cells were cultured as described (Kirshenbaum et al., 2003; Radinger et al., 2010) in StemPro-34 medium containing 13 ml of StemPro-34 Nutrient Supplement and L-glutamine (2 mM) and penicillin (100 U/ml)/streptomycin (100 μg/ml; all from GIBCO, Grand Island, NY) with 100 ng/ml recombinant human SCF added (Peprotech, Rocky Hill, NJ). Half of the medium supplemented with SCF was changed every 7 d. HLMCs were obtained by lung resection for bronchial carcinoma and purified using immunoaffinity magnetic selection using anti-CD117 (BD Biosciences, San Jose, CA) as described (Sanmugalingam et al., 2000) and were cultured as described (Cruse et al., 2008). All human subjects gave written informed consent, and the study was approved by the Leicestershire Research Ethics Committee, United Kingdom. Human peripheral blood–derived mast cells were cultured from CD34+ progenitors as described (Radinger et al., 2010). The donors provided an informed consent, and cells were obtained under a protocol (NCT00001756) approved by the National Institute of Allergy and Infectious Diseases, National Institutes of Health Internal Review Board.

MS4A4 cloning

Total RNA was isolated from 2×10^6 human lung mast cells and LAD-2 cells using the RNEasy kit, which was used according to the

manufacturer's instructions (Qiagen, Valencia, CA). Primers were designed to amplify the full open reading frame of MS4A4 isoforms 1 and 2. cDNA was amplified as described (Cruse *et al.*, 2010). The primers used for cloning were as follows. For isoform 1, forward, GGGGAATTCATGCATCAGACCTACAGCAGAC, and reverse, GGGGGATCCTCAAACCTCATTAAGTGGTGTGG. For isoform 2, forward, GGGGAATTCATGACAACCATGCAAGGAATGGAAC, and reverse, GGGGGATCCTCAAACCTCATTAAGTGGTGTGG.

Only isoform 2 primers amplified a product. The resulting product was gel purified and cloned into the pGEM T Easy Vector System (Promega) and then positively selected and sequenced as described (Cruse *et al.*, 2010). MS4A4 clones were then PCR amplified with high-fidelity DNA polymerase to remove the stop codon and restriction sites *Sac*I and *Sac*II added to the 5′ and 3′ ends using the following primers: forward, GGGGAG-CTCATGACAACCATGCAAGGAATGGAAC, and reverse, GGGCC-GCGGAACCTCATTAAGTGGTGTGGGAG.

The resulting clones without stop codons were subcloned into pEGFP-N1 to attach EGFP to the C terminus of MS4A4 isoform 2. Final clones were sequenced to confirm correct subcloning.

Lentivirus production and transduction of mast cells

For gene silencing, MISSION shRNA constructs and lentiviruses were used (Sigma-Aldrich) as described (Cruse *et al.*, 2013). The following constructs were purchased:

Scramble shRNA control: SHC002
shMS4A4v1: TRCN0000063624
CCGGCCGTGTATATCGGGTACACAACTCGAGTTGTGTACCC-GATATACACGGTTTTTG
shMS4A4v2: TRCN0000063625
CCGGGAGAAGTTCTTGAAGGGAGAACTCGAGTTCTCCC-TTCAAGAACTTCTCTTTTTG
shMS4A4v3: TRCN0000063626
CCGGCGAGGTAGTCTAGGAATGAATCTCGAGATTCATTCC-TAGACTACCTCGTTTTTG
shMS4A4v4: TRCN0000063627
CCGGCCCACACCACTTAATGAGGTTCTCGAGAACCTCATTA-AGTGGTGTGGGTTTTTG

Plasmid DNA was purified, and lentivirus containing the shRNA plasmids was produced as described (Cruse *et al.*, 2013).

Plasmids

Wild-type monomeric red fluorescent protein (mRFP) Rab5 (pmRFP-C3) construct (Vonderheit and Helenius, 2005) was a gift from Ari Helenius (ETH Zurich; Addgene plasmid 14437). The constitutively active mCherry-Rab5CA(Q79L) (PmCherry-C1; Addgene plasmid 35138) and dominant-negative mCherry-Rab5DN(S34N) (PmCherry-C1; Addgene plasmid 35139) were gifts from Sergio Grinstein (University of Toronto; Bohdanowicz *et al.*, 2012). The DsRed-Rab7 WT (pDsRed-C1; Addgene plasmid 12661), DsRed-Rab9 WT (pDsRed-C1; Addgene plasmid 12677), and DsRed-Rab11 WT (pDsRed-C1; Addgene plasmid 12679) were gifts from Richard Pagano (Mayo Clinic; Choudhury *et al.*, 2002).

Transfection of LAD-2 cells

Transfections with cDNA were carried out using the Nucleofector II machine (Amaxa, Anaheim, CA) as described (Cruse *et al.*, 2013). Confocal microscopy with cotransfected live cells was carried out at 16 h posttransfection. For colocalization of MS4A4 and Rab5 variants in Figure 4A, imaging was performed at 6 h posttransfection

due to apparent cytotoxicity of dominant-negative Rab5 expression with the longer incubation.

Quantitative real-time PCR

Primers were designed for MS4A4. Quantitative real-time PCR (qRT-PCR) performed in the United Kingdom (Figure 1C) was carried out using the Full Velocity SYBR Green QRT-PCR system (Stratagene, La Jolla, CA) as described (Cruse *et al.*, 2008). Products were also run on a 1.5% agarose gel to confirm that the products were the expected length. Bands were then excised from the gel and sequenced (Protein and Nucleic Acids Chemistry Laboratory, University of Leicester, Leicester, United Kingdom).

qRT-PCR in the United States (Figure 1, D, E, and L) was carried out as described (Cruse *et al.*, 2013). Total RNA was isolated using the RNeasy Plus kit (Qiagen), which eliminates genomic DNA. Total RNA was reverse transcribed into cDNA using the QuantiTect reverse transcription system (Qiagen), which includes a DNase step to further ensure genomic DNA elimination. The qPCR was carried out using the Quantifast SYBR green kit (Qiagen) on the ABI 7500 machine. Primers were the same for all qPCR: forward, GCATGGGAATA-ACAATGATGTG; and reverse, TCCTAGACTACCTCGGACCAG.

Immunoblotting

LAD-2 cells were incubated overnight in LAD-2 medium without SCF. Cells were then washed twice in 4-(2-hydroxyethyl)-1-piperazineethanesulfonic acid (HEPES) buffer containing 0.04% bovine serum albumin (BSA) and resuspended at 2.5×10^6 cells/ml HEPES buffer containing 0.04% BSA. The cells were challenged with SCF for the indicated time points and then immediately lysed as described (Cruse *et al.*, 2013). Immunoblots were then carried out on the total cell lysates as described (Cruse *et al.*, 2013). The acquired images were analyzed, and densitometry was performed using ImageJ software, version 1.32. For signaling experiments in Figure 2, IRDye (680RD or 800CW)–labeled secondary antibodies (1:20,000) were used to label both phosphorylated and total proteins simultaneously. Membranes were visualized and quantified using an Odyssey CLx imager (LI-COR Biosciences, Lincoln, NE).

Immunoprecipitation

LAD-2 cells were deprived of SCF for 16 h before experiments. Cells were then either left unstimulated or stimulated with SCF for 10 min, followed by plunging into ice. Cells were washed in ice-cold phosphate-buffered saline (PBS) and lysed for 1 h in 1% Triton X immunoprecipitation buffer as described (Cruse *et al.*, 2013). The lysates were then centrifuged at $20,000 \times g$ for 10 min to remove insoluble material. A 50-μl amount of protein A/G UltraLink resin (Thermo Scientific, Waltham, MA) was used to preclear the lysates for 30 min at 4°C with rotation. After preclearing, the lysates were centrifuged at $15,000 \times g$ for 2 min to remove the resin. A 5-μg amount of mouse polyclonal anti-MS4A4 or mouse IgG control was added to the lysates and incubated overnight at 4°C with rotation. Then 50 μl of protein A/G UltraLink resin was added to the lysates and incubated for 3 h at 4°C. The lysates were washed five times in immunoprecipitation buffer. The coimmunoprecipitations were then eluted from the resin with boiling in SDS running buffer as described (Cruse *et al.*, 2013).

Flow cytometry

To assay surface expression of receptors, we used flow cytometric analysis on the FACSCalibur machine (BD Biosciences).

KIT internalization assays

KIT internalization assays were performed on LAD-2 HuMC transduced with either shMS4A4 or scramble shRNA control as described (Cruse et al., 2013). Before the assay, LAD-2 HuMCs at day 7 postinfection with shRNA constructs were washed to remove SCF and incubated overnight (16 h) in cytokine-free LAD-2 HuMC medium. Brefeldin A (BFA) was added and incubated for 2 h at 37°C before experiments in which it was used. Cells were then washed twice in prewarmed (37°C) HEPES buffer (10 mM HEPES, 137 mM NaCl, 2.7 mM KCl, 0.4 mM $Na_2HPO_4\cdot7H_2O$, 5.6 mM glucose, 1.8 mM $CaCl_2\cdot2H_2O$, and 1.3 mM $MgSO_4\cdot7H_2O$ with 0.04% BSA) and resuspended at 5×10^5 LAD-2 HuMCs/ml in HEPES buffer with or without BFA. Time zero was plunged into ice, and the remaining time points were stimulated with recombinant human SCF and mixed. At the indicated time points, cells were plunged into ice. Samples were maintained on ice and washed twice with ice-cold PBS/1% BSA and stained for surface KIT expression. Surface KIT expression was assessed as described in *Flow cytometry*.

KIT recycling and degradation assays

LAD-2 cells were incubated overnight (16 h) at 37°C in StemPro medium without SCF. KIT recycling and degradation were assessed using a method modified from Roepstorff et al. (2009) in which cells were kept ice cold throughout the initial steps. Cells were washed twice in cold HEPES buffer containing 0.04% BSA by centrifugation at 4°C, resuspended in the HEPES/BSA buffer, and maintained on ice. The cell suspensions were incubated with either 10 ng/ml or 100 ng/ml SCF for 1 h on ice. After the incubation, cells were washed three times in the cold HEPES/BSA buffer by centrifugation at 4°C, resuspended in the HEPES/BSA buffer, and divided into precooled fluorescence-activated cell sorting (FACS) tubes (5×10^5 LAD-2 cells in 1 ml/tube) for each time point. Tubes were transferred to a 37°C water bath and transferred back to the ice-water bath at the indicated time points. The 0-min samples were never removed from the ice-water bath. Samples were centrifuged at 4°C and washed once in the HEPES/BSA buffer. Cells were then maintained on ice, and surface staining of KIT was performed as described in *Flow cytometry*.

For each set of stimulations, a subset of cells was incubated for 30 min in 10 µM cycloheximide in 0.1% DMSO before dividing into FACS tubes and warming to 37°C for the indicated time points. Cycloheximide was present for the duration of the assays to prevent repopulation with newly synthesized KIT. At each time point, cells were immersed in an ice-water bath for 10 min before centrifugation and washed once in cold PBS. Cells were then fixed in ice-cold 4% paraformaldehyde (PFA) for 30 min on ice and washed twice in cold PBS. Cells were permeabilized in PBS containing 0.1% saponin for 30 min on ice before staining for total KIT in PBS containing 0.1% saponin and analysis by flow cytometry.

Confocal microscopy and image analysis

Confocal microscopy was carried out within the Biological Imaging Section of the Research Technologies Branch, National Institute of Allergy and Infectious Diseases, National Institutes of Health, on a Leica TCS SP8 confocal microscope. For immunofluorescence analyses, cells were fixed in ice-cold 4% PFA for 30 min on ice, washed twice in cold PBS, and permeabilized in PBS containing 0.1% Triton X for 30 min on ice before staining. Images were collected using a 63× oil immersion objective (numerical aperture [NA] 1.4). Fluorochromes were excited using an argon laser at 488 nm for EGFP and Alexa 488, a helium–neon laser at 568 for RFP, mCherry, DsRed, and Alexa 568, a helium–neon laser at 594 nm for Alexa 594, and a helium–neon laser at 633 for APC and Alexa 647. 4′,6-Diamidino-2-phenylindole was excited using an ultraviolet 405 laser. Sequential images at 200-nm intervals were collected sequentially and superimposed. Imaris software was used for colocalization analyses using automatic thresholding. For live-cell imaging, LAD-2 HuMCs were cotransfected with pEGFP-N1:MS4A4 and red fluorescent–tagged Rab proteins (see *Plasmids*). Cells were plated into eight-well chambered coverglass in HEPES buffer (described earlier) and imaged on a heated stage (37°C) flushed with 5% CO_2. A 63× glycerol immersion objection (NA 1.3) was used, which was also heated to 37°C. Images were collected simultaneously with detector slits configured to minimize any cross-talk between the channels. Images were acquired using Leica LAS AF software and processed using Bitplane Imaris and Huygens Essential software. For colocalization analyses, the Bitplane Imaris colocalization analysis tool was used on unprocessed image stacks.

Apoptosis assays

For the analysis of apoptosis. Fluorescein isothiocyanate–conjugated annexin V (BD PharMingen) and propidium iodide were used as described (Cruse et al., 2010).

Mast cell proliferation and migration assays

Mast cell proliferation was determined by incubation of transduced LAD-2 mast cells in complete StemPro medium with 100 ng/ml SCF in 12-well plates (5×10^5 cells/well). Duplicate wells were counted by flow cytometry at the indicated time points, and nonviable cells were identified by staining with propidium iodide and eliminated from the analysis. Mast cell migration was assessed as described (Cruse et al., 2006, 2011).

Statistical analysis

For comparison of multiple data sets, one- or two-way ANOVA with Bonferroni's, Sidak's, or Tukey's posttest were used, as appropriate, to determine statistical significance. For pairwise data, Student's *t* test was used. $p\leq0.05$ was considered statistically significant.

REFERENCES

Abram CL, Courtneidge SA (2000). Src family tyrosine kinases and growth factor signaling. Exp Cell Res 254, 1–13.

Arcaro A, Aubert M, Espinosa del Hierro ME, Khanzada UK, Angelidou S, Tetley TD, Bittermann AG, Frame MC, Seckl MJ (2007). Critical role for lipid raft-associated Src kinases in activation of PI3K-Akt signalling. Cell Signal 19, 1081–1092.

Bangur CS, Johnson JC, Switzer A, Wang YH, Hill B, Fanger GR, Wang T, Retter MW (2004). Identification and characterization of L985P, a CD20 related family member over-expressed in small cell lung carcinoma. Int J Oncol 25, 1583–1590.

Blachly JS, Baiocchi RA (2014). Targeting the PI3-kinase (PI3K), AKT and mTOR axis in lymphoma. Br J Pharmacol 167, 19–31.

Blume-Jensen P, Claesson-Welsh L, Siegbahn A, Zsebo KM, Westermark B, Heldin CH (1991). Activation of the human c-kit product by ligand-induced dimerization mediates circular actin reorganization and chemotaxis. EMBO J 10, 4121–4128.

Bohdanowicz M, Balkin DM, De Camilli P, Grinstein S (2012). Recruitment of OCRL and Inpp5B to phagosomes by Rab5 and APPL1 depletes phosphoinositides and attenuates Akt signaling. Mol Biol Cell 23, 176–187.

Brankatschk B, Wichert SP, Johnson SD, Schaad O, Rossner MJ, Gruenberg J (2012). Regulation of the EGF transcriptional response by endocytic sorting. Sci Signal 5, ra21.

Burke P, Schooler K, Wiley HS (2001). Regulation of epidermal growth factor receptor signaling by endocytosis and intracellular trafficking. Mol Biol Cell 12, 1897–1910.

Choudhury A, Dominguez M, Puri V, Sharma DK, Narita K, Wheatley CL, Marks DL, Pagano RE (2002). Rab proteins mediate Golgi transport of caveola-internalized glycosphingolipids and correct lipid trafficking in Niemann-Pick C cells. J Clin Invest 109, 1541–1550.

Cruse G, Beaven MA, Ashmole I, Bradding P, Gilfillan AM, Metcalfe DD (2013). A truncated splice-variant of the FcepsilonRIbeta receptor subunit is critical for microtubule formation and degranulation in mast cells. Immunity 38, 906–917.

Cruse G, Cockerill S, Bradding P (2008). IgE alone promotes human lung mast cell survival through the autocrine production of IL-6. BMC Immunol 9, 2.

Cruse G, Duffy SM, Brightling CE, Bradding P (2006). Functional KCa3.1 K+ channels are required for human lung mast cell migration. Thorax 61, 880–885.

Cruse G, Kaur D, Leyland M, Bradding P (2010). A novel FcepsilonRIbeta-chain truncation regulates human mast cell proliferation and survival. FASEB J 24, 4047–4057.

Cruse G, Singh S, Duffy SM, Doe C, Saunders R, Brightling CE, Bradding P (2011). Functional KCa3.1 K +channels are required for human fibrocyte migration. J Allergy Clin Immunol 128, 1303–1309.

Dalerba P, Kalisky T, Sahoo D, Rajendran PS, Rothenberg ME, Leyrat AA, Sim S, Okamoto J, Johnston DM, Qian D, et al. (2011). Single-cell dissection of transcriptional heterogeneity in human colon tumors. Nat Biotechnol 29, 1120–1127.

Donato JL, Ko J, Kutok JL, Cheng T, Shirakawa T, Mao XQ, Beach D, Scadden DT, Sayegh MH, Adra CN (2002). Human HTm4 is a hematopoietic cell cycle regulator. J Clin Invest 109, 51–58.

Goh LK, Sorkin A (2013). Endocytosis of receptor tyrosine kinases. Cold Spring Harb Perspect Biol 5, a017459.

Grant BD, Donaldson JG (2009). Pathways and mechanisms of endocytic recycling. Nat Rev Mol Cell Biol 10, 597–608.

Halova I, Draberova L, Draber P (2012). Mast cell chemotaxis—chemoattractants and signaling pathways. Front Immunol 3, 119.

Haugh JM, Meyer T (2002). Active EGF receptors have limited access to PtdIns(4,5)P(2) in endosomes: implications for phospholipase C and PI 3-kinase signaling. J Cell Sci 115, 303–310.

Hollingworth P, Harold D, Sims R, Gerrish A, Lambert JC, Carrasquillo MM, Abraham R, Hamshere ML, Pahwa JS, Moskvina V, et al. (2011). Common variants at ABCA7, MS4A6A/MS4A4E, EPHA1, CD33 and CD2AP are associated with Alzheimer's disease. Nat Genet 43, 429–435.

Howie D, Nolan KF, Daley S, Butterfield E, Adams E, Garcia-Rueda H, Thompson C, Saunders NJ, Cobbold SP, Tone Y, et al. (2009). MS4A4B is a GITR-associated membrane adapter, expressed by regulatory T cells, which modulates T cell activation. J Immunol 183, 4197–4204.

Huotari J, Helenius A (2011). Endosome maturation. EMBO J 30, 3481–3500.

Hu J, Troglio F, Mukhopadhyay A, Everingham S, Kwok E, Scita G, Craig AW (2009). F-BAR-containing adaptor CIP4 localizes to early endosomes and regulates epidermal growth factor receptor trafficking and downregulation. Cell Signal 21, 1686–1697.

Ishibashi K, Suzuki M, Sasaki S, Imai M (2001). Identification of a new multigene four-transmembrane family (MS4A) related to CD20, HTm4 and beta subunit of the high-affinity IgE receptor. Gene 264, 87–93.

Jahn T, Leifheit E, Gooch S, Sindhu S, Weinberg K (2007). Lipid rafts are required for Kit survival and proliferation signals. Blood 110, 1739–1747.

Jensen BM, Metcalfe DD, Gilfillan AM (2007). Targeting kit activation: a potential therapeutic approach in the treatment of allergic inflammation. Inflamm. Allergy Drug Targets 6, 57–62.

Kageyama-Yahara N, Suehiro Y, Yamamoto T, Kadowaki M (2011). Rab5a regulates surface expression of FcepsilonRI and functional activation in mast cells. Biol Pharm Bull 34, 760–763.

Kalesnikoff J, Rios EJ, Chen CC, Alejandro Barbieri M, Tsai M, Tam SY, Galli SJ (2007). Roles of RabGEF1/Rabex-5 domains in regulating Fc epsilon RI surface expression and Fc epsilon RI-dependent responses in mast cells. Blood 109, 5308–5317.

Kermorgant S, Parker PJ (2008). Receptor trafficking controls weak signal delivery: a strategy used by c-Met for STAT3 nuclear accumulation. J Cell Biol 182, 855–863.

Kirshenbaum AS, Akin C, Wu Y, Rottem M, Goff JP, Beaven MA, Rao VK, Metcalfe DD (2003). Characterization of novel stem cell factor responsive human mast cell lines LAD 1 and 2 established from a patient with mast cell sarcoma/leukemia; activation following aggregation of FcepsilonRI or FcgammaRI. Leuk Res 27, 677–682.

Kolch W (2000). Meaningful relationships: the regulation of the Ras/Raf/MEK/ERK pathway by protein interactions. Biochem J 351, 289–305.

Kon S, Minegishi N, Tanabe K, Watanabe T, Funaki T, Wong WF, Sakamoto D, Higuchi Y, Kiyonari H, Asano K, et al. (2013). Smap1 deficiency perturbs receptor trafficking and predisposes mice to myelodysplasia. J Clin Invest 123, 1123–1137.

Koslowski M, Sahin U, Dhaene K, Huber C, Tureci O (2008). MS4A12 is a colon-selective store-operated calcium channel promoting malignant cell processes. Cancer Res 68, 3458–3466.

Kovarova M, Tolar P, Arudchandran R, Draberova L, Rivera J, Draber P (2001). Structure-function analysis of Lyn kinase association with lipid rafts and initiation of early signaling events after Fcepsilon receptor I aggregation. Mol Cell Biol 21, 8318–8328.

Kraft S, Rana S, Jouvin MH, Kinet JP (2004). The role of the FcepsilonRI beta-chain in allergic diseases. Int Arch Allergy Immunol 135, 62–72.

Kranenburg O, Verlaan I, Moolenaar WH (1999). Dynamin is required for the activation of mitogen-activated protein (MAP) kinase by MAP kinase kinase. J Biol Chem 274, 35301–35304.

Kutok JL, Yang X, Folkerth R, Adra CN (2011). Characterization of the expression of HTm4 (MS4A3), a cell cycle regulator, in human peripheral blood cells and normal and malignant tissues. J Cell Mol Med 15, 86–93.

Lajoie P, Nabi IR (2010). Lipid rafts, caveolae, and their endocytosis. Int Rev Cell Mol Biol 282, 135–163.

Liang Y, Buckley TR, Tu L, Langdon SD, Tedder TF (2001). Structural organization of the human MS4A gene cluster on Chromosome 11q12. Immunogenetics 53, 357–368.

Liang Y, Tedder TF (2001). Identification of a CD20-, FcepsilonRIbeta-, and HTm4-related gene family: sixteen new MS4A family members expressed in human and mouse. Genomics 72, 119–127.

Linnekin D, DeBerry CS, Mou S (1997). Lyn associates with the juxtamembrane region of c-Kit and is activated by stem cell factor in hematopoietic cell lines and normal progenitor cells. J Biol Chem 272, 27450–27455.

Ma P, Mali RS, Munugalavadla V, Krishnan S, Ramdas B, Sims E, Martin H, Ghosh J, Li S, Chan RJ, et al. (2011). The PI3K pathway drives the maturation of mast cells via microphthalmia transcription factor. Blood 118, 3459–3469.

Maxfield FR, McGraw TE (2004). Endocytic recycling. Nat Rev Mol Cell Biol 5, 121–132.

Michel J, Schonhaar K, Schledzewski K, Gkaniatsou C, Sticht C, Kellert B, Lasitschka F, Geraud C, Goerdt S, Schmieder A (2013). Identification of the novel differentiation marker MS4A8B and its murine homolog MS4A8A in colonic epithelial cells lost during neoplastic transformation in human colon. Cell Death Dis 4, e469.

Mizuno-Yamasaki E, Rivera-Molina F, Novick P (2012). GTPase networks in membrane traffic. Annu Rev Biochem 81, 637–659.

Naj AC, Jun G, Beecham GW, Wang LS, Vardarajan BN, Buros J, Gallins PJ, Buxbaum JD, Jarvik GP, Crane PK, et al. (2011). Common variants at MS4A4/MS4A6E, CD2AP, CD33 and EPHA1 are associated with late-onset Alzheimer's disease. Nat Genet 43, 436–441.

Obata Y, Toyoshima S, Wakamatsu E, Suzuki S, Ogawa S, Esumi H, Abe R (2014). Oncogenic Kit signals on endolysosomes and endoplasmic reticulum are essential for neoplastic mast cell proliferation. Nat Commun 5, 5715.

Okayama Y, Kawakami T (2006). Development, migration and survival of MCs. Immunol Res 34, 97–115.

Palfy M, Remenyi A, Korcsmaros T (2012). Endosomal crosstalk: meeting points for signaling pathways. Trends Cell Biol 22, 447–456.

Parachoniak CA, Luo Y, Abella JV, Keen JH, Park M (2011). GGA3 functions as a switch to promote Met receptor recycling, essential for sustained ERK and cell migration. Dev Cell 20, 751–763.

Pawson T (2004). Specificity in signal transduction: from phosphotyrosine-SH2 domain interactions to complex cellular systems. Cell 116, 191–203.

Platta HW, Stenmark H (2011). Endocytosis and signaling. Curr Opin Cell Biol 23, 393–403.

Poteryaev D, Datta S, Ackema K, Zerial M, Spang A (2010). Identification of the switch in early-to-late endosome transition. Cell 141, 497–508.

Radinger M, Jensen BM, Kuehn HS, Kirshenbaum A, Gilfillan AM (2010). Generation, isolation, and maintenance of human mast cells and mast cell lines derived from peripheral blood or cord blood. Curr Protoc Immunol Chapter 7, Unit 7.37.

Rios EJ, Piliponsky AM, Ra C, Kalesnikoff J, Galli SJ (2008). Rabaptin-5 regulates receptor expression and functional activation in mast cells. Blood 112, 4148–4157.

Roepstorff K, Grandal MV, Henriksen L, Knudsen SL, Lerdrup M, Grøvdal L, Willumsen BM, van Deurs B (2009). Differential effects of EGFR ligands on endocytic sorting of the receptor. Traffic 10, 1115–27.

Ronnstrand L (2004). Signal transduction via the stem cell factor receptor/c-Kit. Cell Mol Life Sci 61, 2535–2548.

Sanmugalingam D, Wardlaw AJ, Bradding P (2000). Adhesion of human lung mast cells to bronchial epithelium: evidence for a novel carbohydrate-mediated mechanism. J Leukoc Biol 68, 38–46.

Scita G, Di Fiore PP (2010). The endocytic matrix. Nature 463, 464–473.

Sigismund S, Argenzio E, Tosoni D, Cavallaro E, Polo S, Di Fiore PP (2008). Clathrin-mediated internalization is essential for sustained EGFR signaling but dispensable for degradation. Dev Cell 15, 209–219.

Smrž D., Bandara G, Beaven MA, Metcalfe DD, Gilfillan AM (2013). Prevention of F-actin assembly switches the response to SCF from chemotaxis to degranulation in human mast cells. Eur J Immunol 43, 1873–1882.

Stenmark H (2009). Rab GTPases as coordinators of vesicle traffic. Nat Rev Mol Cell Biol 10, 513–525.

Stenmark H, Parton RG, Steele-Mortimer O, Lutcke A, Gruenberg J, Zerial M (1994). Inhibition of rab5 GTPase activity stimulates membrane fusion in endocytosis. EMBO J 13, 1287–1296.

Taub N, Teis D, Ebner HL, Hess MW, Huber LA (2007). Late endosomal traffic of the epidermal growth factor receptor ensures spatial and temporal fidelity of mitogen-activated protein kinase signaling. Mol Biol Cell 18, 4698–4710.

Tedder TF, Engel P (1994). CD20: a regulator of cell-cycle progression of B lymphocytes. Immunol Today 15, 450–454.

Teis D, Taub N, Kurzbauer R, Hilber D, de Araujo ME, Erlacher M, Offterdinger M, Villunger A, Geley S, Bohn G, et al. (2006). p14-MP1-MEK1 signaling regulates endosomal traffic and cellular proliferation during tissue homeostasis. J Cell Biol 175, 861–868.

Teis D, Wunderlich W, Huber LA (2002). Localization of the MP1-MAPK scaffold complex to endosomes is mediated by p14 and required for signal transduction. Dev Cell 3, 803–814.

Toffalini F, Demoulin JB (2010). New insights into the mechanisms of hematopoietic cell transformation by activated receptor tyrosine kinases. Blood 116, 2429–2437.

van der Geer P, Hunter T, Lindberg RA (1994). Receptor protein-tyrosine kinases and their signal transduction pathways. Annu Rev Cell Biol 10, 251–337.

Vieira AV, Lamaze C, Schmid SL (1996). Control of EGF receptor signaling by clathrin-mediated endocytosis. Science 274, 2086–2089.

Vonderheit A, Helenius A (2005). Rab7 associates with early endosomes to mediate sorting and transport of Semliki forest virus to late endosomes. PLoS Biol 3, e233.

Woodman PG (2000). Biogenesis of the sorting endosome: the role of Rab5. Traffic 1, 695–701.

Wu P, Wee P, Jiang J, Chen X, Wang Z (2012). Differential regulation of transcription factors by location-specific EGF receptor signaling via a spatio-temporal interplay of ERK activation. PLoS One 7, e41354.

Xiang Z, Kreisel F, Cain J, Colson A, Tomasson MH (2007). Neoplasia driven by mutant c-KIT is mediated by intracellular, not plasma membrane, receptor signaling. Mol Cell Biol 27, 267–282.

Xu H, Williams MS, Spain LM (2006). Patterns of expression, membrane localization, and effects of ectopic expression suggest a function for MS4a4B, a CD20 homolog in Th1 T cells. Blood 107, 2400–2408.

Xu H, Yan Y, Williams MS, Carey GB, Yang J, Li H, Zhang GX, Rostami A (2010). MS4a4B, a CD20 homologue in T cells, inhibits T cell propagation by modulation of cell cycle. PLoS One 5, e13780.

Yan Y, Li Z, Zhang GX, Williams MS, Carey GB, Zhang J, Rostami A, Xu H (2013). Anti-MS4a4B treatment abrogates MS4a4B-mediated protection in T cells and ameliorates experimental autoimmune encephalomyelitis. Apoptosis 18, 1106–1119.